JREE: Vol. 12, No. 4, (Autumn 2025) 81-88

Journal of Renewable Energy and Environment

Journal Homepage: www.jree.ir

Materials and Energy Research Center

MERC

Research Article

Ecofriendly Dye Sensitized Solar Cell Based on PEO/Graphite Nanofiller for Long Term Stability

Kumari Pooja[a], Shivansh Tripathi[b], Anshu Maurya[a], Priyanka Chawla[a], Mridula Tripathi[a]*

[a] Department of Chemistry, College of CMP Degree, University of Allahabad, Prayagraj, Uttar Pradesh, India.
[b] Department of Space, Laboratory of National Atmospheric Research, Government of India, Tirupati, Andhra Pradesh, India.

PAPER INFO

Paper history:
Received: 05 January 2025
Revised: 20 June 2025
Accepted: 21 September 2025

Keywords:
Polyethylene Oxide (PEO),
Polymer Electrolyte,
Dye Sensitized Solar Cell (DSSC),
Filler,
Graphite,
TiO2-CuO,
Cocktail Dye

ABSTRACT

This study reports the development of a novel and eco-friendly dye-sensitized solar cell (DSSC) through the modification of its three major components: sensitizer, electrolyte, and photoanode. A natural cocktail dye was employed as the sensitizer, a polymer electrolyte with graphite filler as the electrolyte, and a TiO_2–CuO nanocomposite as the photoanode. Natural dyes extracted from Beta vulgaris (beetroot) and Spinacia oleracea (spinach) were mixed in a 1:1 v/v ratio to form a cocktail sensitizer, thereby enhancing the absorption properties and light-harvesting efficiency of the device. The polymer electrolyte was fabricated via the solution casting technique using polyethylene oxide (PEO) as the host matrix, lithium iodide/iodine (LiI/I_2) as the redox couple, ethylene carbonate (EC) and propylene carbonate (PC) as plasticizers, and graphite as a conductive nanofiller. Owing to its excellent electrical conductivity, thermal stability, and low cost, graphite significantly improved the ionic conductivity of the electrolyte to 10^{-3} S/cm. A TiO_2–CuO nanocomposite was synthesized using the sol–gel method and employed as the photoanode material, which improved electron transport and reduced recombination losses due to the synergistic effects between TiO_2 and CuO. Structural characterization was performed using Fourier Transform Infrared Spectroscopy (FTIR) and X-ray Diffraction (XRD). The fabricated DSSC exhibited a power conversion efficiency of 3.3%, with a short-circuit current density (Jsc) of 9.0 mA/cm², an open-circuit voltage (Voc) of 0.68 V, and a fill factor of 57%. This multi-component modification combining sustainable natural dyes, a low-cost graphite-based solid polymer electrolyte, and a TiO_2–CuO nanocomposite photoanode offers a promising strategy for enhancing DSSC performance while maintaining both environmental and economic viability.

https://doi.org/10.30501/jree.2025.486998.2151

1. INTRODUCTION

Polymer electrolytes have emerged as promising materials for a wide range of electrochemical devices, including sensors, solid-state rechargeable batteries, dye-sensitized solar cells (DSSCs), supercapacitors, and electrochromic windows (Ngai et al., 2016; Tripathi & Chawla, 2015; Lu et al., 2023; T. K. & Saratha, 2024; Hao et al., 2024). Their advantages include excellent mechanical stability, strong electrode–electrolyte interactions, flexible processability, and, most importantly, their leak-proof nature compared to liquid electrolytes (Lv et al., 2024; Zhao et al., 2021). However, polymer electrolytes generally exhibit lower ionic conductivity than their liquid counterparts, which remains a critical limitation. To overcome this drawback, researchers have investigated the incorporation of various metal salts and conductive non-metallic fillers such as graphite, carbon nanotubes, and graphene into polymer hosts, effectively enhancing both ionic conductivity and mechanical performance (Sangwan et al., 2023; Pooja et al., 2021; Bathaei et al., 2022; Dissanayake et al., 2024).

In this work, we employed polyethylene oxide (PEO) as the host polymer and graphite as the filler material. PEO is a semicrystalline, non-toxic thermoplastic polymer that contains both crystalline and amorphous phases at room temperature. It possesses coordinating ether oxygen atoms in its backbone, which facilitate ionic conduction through Lewis acid–base interactions with cations and the segmental mobility of polymer chains. While the crystalline regions provide structural integrity, the amorphous regions primarily support ion transport, making the enhancement of amorphous phases a key strategy for improving conductivity (Ida & Suthanthiraraj, 2019; Dissanayake et al., 2016; Nogueira et al., 2001; Nei de Freitas et al., 2009). These properties make PEO highly suitable for use as a polymer electrolyte.

Graphite, an abundant and naturally occurring form of crystalline carbon, exhibits excellent electrical conductivity (~10^{-4} S/cm at room temperature), thermal stability, and strong compatibility with polymers. Its planar layered structure allows for the intercalation of charge carriers, and its compatibility with organic matrices makes it an ideal choice as a conductive filler (Cermak et al., 2020; Coetzee et al., 2023). Additional advantages of graphite include high energy and power density, long cycle life, and low cost, making it particularly suitable for

*Corresponding Author's Email: mtcmpau@gmail.com (M. Tripathi)
URL: https://www.jree.ir/article_229950.html

Please cite this article as: Pooja, K., Tripathi, S., Maurya, A., Chawla, P. & Tripathi, M. (2025). Ecofriendly Dye Sensitized Solar Cell Based on PEO/Graphite Nanofiller for Long Term Stability. *Journal of Renewable Energy and Environment (JREE)*, 12(4), 81-88. https://doi.org/10.30501/jree.2025.486998.2151.

sustainable DSSC fabrication (Zhang et al., 2021; Mao et al., 2018; Hebali et al., 2024).

Dye-sensitized solar cells (DSSCs) have attracted considerable attention from both academia and industry as a potential sustainable energy solution since Grätzel's seminal work in 1991 (Grätzel, 2001). Previous studies have demonstrated that natural dyes and polymer electrolytes can be effectively employed in DSSC fabrication. In the present study, we used a natural cocktail dye—a blend of two dyes—as the sensitizer. Recognizing the critical role of the photoanode in determining overall device efficiency, we modified the conventional TiO_2 anode by synthesizing a TiO_2–CuO composite, which was then employed as the photoanode. Figure 1 depicts a schematic representation of a typical DSSC.

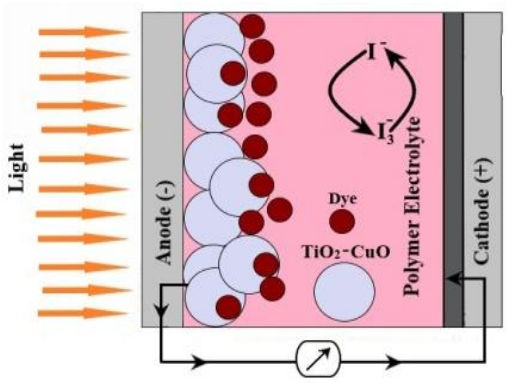

Figure 1. Schematic diagram of a dye sensitized solar cell

TiO_2 can capture only about 6% of the entire solar irradiation due to its wide band gap of 3.2 eV. To overcome this limitation, research has demonstrated that incorporating additional metal oxides such as tin(IV) oxide (SnO_2), zinc oxide (ZnO), and tungsten trioxide (WO_3) can enhance the photocatalytic and photoelectrolytic properties of TiO_2. Among these, CuO has attracted significant attention owing to its unique physical properties and diverse applications, including gas sensing, as well as photochromic and electrochromic devices (Khan & Sahai, 2024; Pooja et al., 2022; Khan & Shah, 2023; Anucha et al., 2022; Krishnan et al., 2024). CuO is particularly suitable for modifying the TiO_2 photoelectrode because it can form a p–n junction with TiO_2, which effectively facilitates the separation of photogenerated charge carriers. The appropriate electrical potential at the TiO_2/CuO interface promotes this separation: electrons from the conduction band of TiO_2 are transferred into the CuO conduction band, while holes accumulate in the valence band. This process reduces recombination losses and enhances charge separation, thereby improving the overall efficiency of the photoelectrode (Chawla et al., 2022; Kohestani & Ezoji, 2021; Shin et al., 2006).

Utilizing a polymer electrolyte system composed of PEO as the host polymer, LiI/I_2 as the redox couple, ethylene carbonate (EC) and propylene carbonate (PC) as plasticizers, and graphite as the filler, together with a cocktail dye and a TiO_2 photoanode modified with CuO, we fabricated a DSSC in this study. We investigated the short-circuit photocurrent density (Jsc), open-circuit voltage (Voc), fill factor (FF), power conversion efficiency (PCE), stability, and other performance attributes of the fabricated device.

The primary objective of this work is to demonstrate a novel integration approach that combines the individual advantages of a modified metal oxide photoanode, a natural sensitizer, and a graphite-reinforced polymer electrolyte to develop a high-performance DSSC. This hybrid configuration is expected to significantly enhance light absorption, facilitate faster charge transport, and minimize recombination reactions, all of which are critical for improving overall PCE. Moreover, the use of naturally abundant, non-toxic, and low-cost materials aligns with global priorities in sustainable energy research.

The novelty of this work lies not only in the eco-friendly material selection but also in the synergistic design of the photoanode–electrolyte–dye interface, which is engineered to optimize the functional role of each component. By integrating material sustainability with performance-driven architecture, this study proposes a viable pathway toward scalable, next-generation DSSC technologies.

2. EXPERIMENTAL

2.1 Preparation of polymer electrolyte

The well-established solution casting process was employed to prepare the PEO-based polymer electrolyte film. An appropriate quantity of PEO was dissolved in distilled water to form a thin polymeric layer, into which the LiI/I_2 redox couple was also dissolved. To ensure homogeneity, the solution was continuously stirred for 6–8 hours. The homogeneous mixture was then combined with ethylene carbonate (EC), propylene carbonate (PC), and graphite nanopowder, followed by overnight blending. Graphite nanopowder was prepared by ball milling the raw material in a planetary ball mill for 48 hours at 300 rpm, using the Retsch PM 100 technique. Finally, the mixture of PEO, LiI/I_2, graphite, EC, and PC was poured into a polypropylene dish. The solvent was slowly evaporated at room temperature, and the resulting film was vacuum-dried to obtain a solvent-free polymer electrolyte sheet. Figure 2 illustrates the preparation process of the polymer electrolyte.

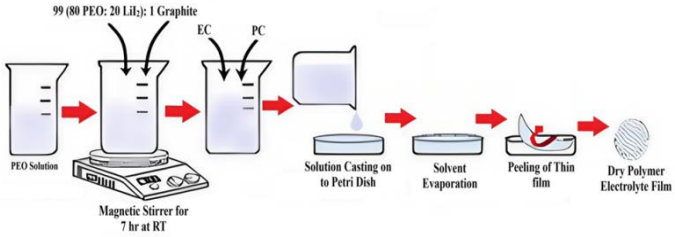

Figure 2. Polymer electrolyte synthesis

2.2 Extraction and purification of dye

Fifty grams of fresh Spinacia oleracea (spinach) leaves and fifty grams of Beta vulgaris (beetroot) fragments were washed with deionized water and subsequently pulverized in a mortar. Each sample was then immersed in 100 mL of ethanol in separate beakers for one week. After filtration, the resulting solutions were concentrated using a rotary evaporator (rotavapor) operated at 40°C. The concentrated dye solutions were combined in a 1:1 volume ratio to prepare the natural cocktail dye sensitizer for the DSSC. To further purify the collected dyes, chromatographic methods were employed. Figure 3 shows the extracted dye, while Figure 4 presents a schematic diagram of the chromatographic method used for purifying the dyes isolated from *Beta vulgaris* and *Spinacia oleracea*.

2.3 TiO_2-CuO photoelectrode preparation

The sol–gel method was employed to synthesize TiO_2 and CuO nanopowders. To prepare the TiO_2 colloidal solution, titanium isopropoxide [$Ti(OCH(CH_3)_2)_4$] was added dropwise to propanol. A white precipitate formed upon the addition of deionized water and was allowed to settle for five minutes. Subsequently, 1 mL of 70% HNO_3 was added to the mixture.

After stirring, the solution was heated at 80°C for 15 minutes to allow partial evaporation of propanol and water, resulting in the formation of a TiO_2 colloidal solution. The CuO colloidal solution was prepared by adding 1 mL of glacial acetic acid and 0.2 M $CuCl_2 \cdot 6H_2O$ to an aqueous solution. The mixture was continuously stirred while being heated to 100°C. An 8 M NaOH solution was then added dropwise until the pH reached 7, leading to the formation of a substantial precipitate and yielding a CuO colloidal solution. To synthesize the TiO_2–CuO nanocomposite, the CuO solution was gradually added to the TiO_2 colloidal solution under vigorous stirring for six hours. The resulting gel was dried and subsequently calcined at 450°C to obtain the TiO_2–CuO nanocomposite.

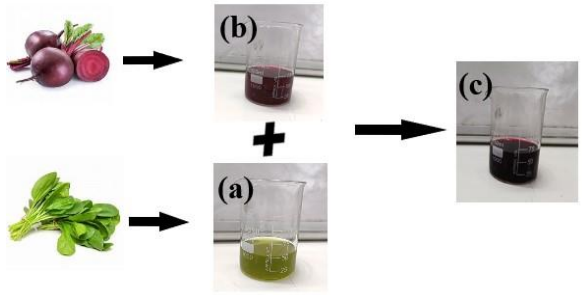

Figure 3. (a) Spinacia oleracea dye (b) Beta vulgaris dye (c) Cocktail dye

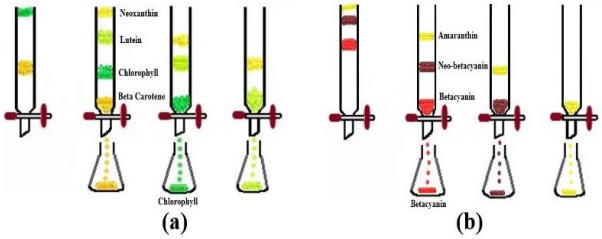

Figure 4. (a) Purification of *Spinacia oleracea* (b) Purification of *Beta vulgaris* via chromatographic technique

2.4 DSSC Fabrication

ITO conductive glass plates were first rinsed with water and ethanol, dried, and then cleaned in an ultrasonic bath containing a detergent solution for 15 minutes. The glass plates had a sheet resistance of 15 Ω/cm². Using the doctor-blade method, TiO_2–CuO nanopastes were applied onto the conductive ITO glass to construct the TiO_2–CuO layer. The resulting film was heated at 150°C for 5–10 minutes. The prepared photoelectrode was subsequently immersed in a Petri dish containing the extracted cocktail dye. The system was kept covered for 24 hours to prevent photodegradation of the dye and left undisturbed during this period. Finally, the fabricated polymer electrolyte was sandwiched between the photoanode and the photocathode, as illustrated in Figure 5. A platinum-based cathode was employed.

2.5 Characterization Techniques

The XRD pattern of the produced polymer electrolyte sheet was recorded at room temperature using a Philips PW 1710 diffractometer within the 2θ range of 20–80°. Electrochemical impedance of the electrolyte film was measured using a Biologic SP-150. Structural and morphological characterization of TiO_2–CuO nanomaterials was carried out using an X-ray diffractometer (Philips PW 1710) equipped with a graphite monochromator and a scanning electron microscope (Carl Zeiss Evo 18). Fourier-transform infrared spectroscopy (FTIR) analysis was performed with a PerkinElmer instrument. The absorbance spectrum of the cocktail dye-coated TiO_2–CuO on ITO was obtained using a double-beam spectrophotometer (Systronics 2201).

DSSC fabrication and performance measurement: The TiO_2–CuO-based photoanode was immersed in the cocktail dye solution (1:1 ratio) for 12 h. The PEO-based polymer electrolyte containing the redox couple was then sandwiched between the dye-sensitized working electrode and the counter electrode to assemble the solar cell. All electrochemical measurements were performed using a Biologic SP-150. A Xenon–Mercury lamp (Oriel Corporation, USA) with an intensity of 100 mW/cm² was used as the light source

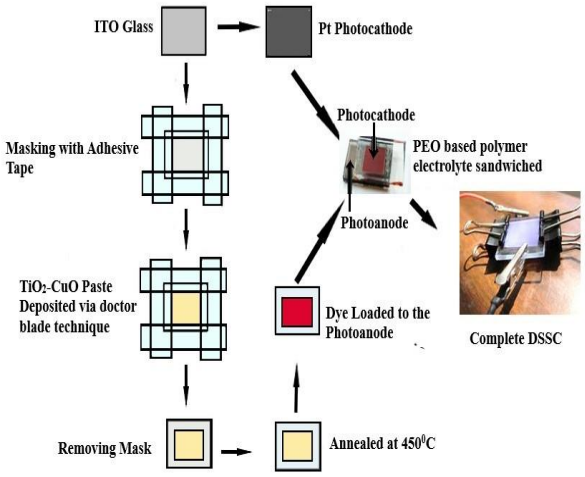

Figure 5. Fabrication of DSSC

3. RESULTS AND DISCUSSION

Figure 6 shows the XRD pattern of a 98{80 PEO–20 LiI/I_2}:2 graphite film prepared via the solution casting process. Sharp, well-defined peaks are observed in the XRD pattern of pure PEO at 19.36° and 23.52°, whereas pure graphite exhibits a characteristic peak at 25°. Comparative analysis of the XRD patterns reveals that the addition of graphite as a filler reduces the intensity of the polymer's main peaks and broadens their widths, indicating an increase in the degree of amorphousness. Intercalation of the polymer chains with the graphite filler expands the interlayer spacing, rendering the film more amorphous overall. This amorphous structure facilitates enhanced ion transport, thereby improving the conductivity of the polymer electrolyte film. At 80× magnification, Figures 7(a) and 7(b) show the surface morphology of 98{80 PEO–20 LiI/I_2}:2 graphite films prepared via the solution casting method. Under the microscope, no discernible PEO spherulite patterns are observed, and the surface roughness is reduced, reflecting a decrease in the crystalline fraction of the polymer. This effect can be attributed to the intercalation of lithium iodide and graphite, which reduces the crystalline character of the host polymer (PEO) and increases the overall amorphous content of the material. Figure 8 presents the FTIR spectra of graphite, pure PEO, and the PEO–graphite composite. Distinct spectral features reveal the structural interactions among the components. In pure PEO (Figure 8a), a broad absorption band is observed between 2950–2700 cm^{-1}, corresponding to the symmetric and asymmetric stretching vibrations of the CH_2 groups. This band becomes narrower in the composite (Figure 8c), indicating restricted polymer chain motion due to interactions with graphite.

The C–O–C symmetric stretching vibration, characteristic of the ether backbone of PEO, appears in the 1050–1150 cm^{-1}

region. Upon incorporation of graphite, this band becomes broader and more intense, suggesting strong intermolecular interactions between PEO chains and the graphite surface. This interaction is attributed to coordination between the oxygen atoms in the ether linkages of PEO and the π-conjugated structure of graphite, which facilitates improved ion transport pathways. The graphite spectrum (Figure 8b) exhibits characteristic vibrational modes, including C=C stretching around 1600 cm^{-1} and a broad band below 1000 cm^{-1}. These bands contribute to the overall spectral profile of the polymer electrolyte system (Figure 8c) and confirm the successful incorporation of graphite into the polymer matrix.

The enhanced vibrational coupling observed in the 1050–1150 cm^{-1} region correlates directly with improved ionic conductivity, as it indicates increased segmental motion and better ion coordination via Lewis acid–base interactions between graphite and PEO chains. These structural modifications underscore the role of graphite as an effective filler for enhancing the electrical performance of the polymer electrolyte system (Wen et al., 1996; Shriver et al., 1981)

Table 1 gives detailed inforations of characteristic peaks corresponding to specific vibration modes, providing insights into polymer–filler interactions. The CH_2 symmetric and asymmetric stretching bands at 2950–2700 cm^{-1} narrow in the PEO–graphite composite, indicating restricted chain mobility due to graphite incorporation (Tsai et al., 2004; Nethravathi & Rajamathi, 2008). Peaks in the 1600–1500 cm^{-1} region, corresponding to C=C stretching of graphite and PEO, confirm successful graphite embedding (Szabó et al., 2006; Chen et al., 2015). The 1150–1050 cm^{-1} C–O–C symmetric stretching band becomes broader and more intense in the composite, reflecting enhanced polymer–filler interaction (Gómez et al., 2021; Arulsankar et al., 2013). The new sharp peaks at ~900–700 cm^{-1}, arising from graphite structural modes, appear exclusively in the composite (Park et al., 2009). These observations collectively indicate that graphite incorporation significantly influences the structural dynamics of the PEO matrix, enhancing polymer–filler interactions.

Figure 9 shows that the ambient AC conductivity of the PEO polymer electrolyte with graphite filler exceeds 10^{-3} S/cm, compared to 0.32×10^{-8} S/cm for pure PEO. The conductivity increases linearly with frequency up to 5 kHz. The AC conductivity of the sample is frequency-dependent, following the well-known power law:

$$\sigma^{ac} = A\omega^{\rho} \quad (1)$$

where A is the constant and ρ is the frequency exponent (ρ<1). The power law (ωρ) is commonly observed in a diverse array of materials, including polymers.

Figure 10 illustrates the light absorption properties of betacyanin, chlorophyll, and the cocktail dye, with each dye exhibiting characteristic absorption peaks corresponding to their molecular structures. Betacyanin predominantly absorbs light at 550 nm, whereas chlorophyll exhibits two prominent absorption peaks at approximately 440 nm and 660 nm.

It is important to note that betacyanin exhibits minimal absorption at 660 nm, a wavelength where chlorophyll shows significant absorption. The enhanced absorption at 660 nm in the cocktail dye is primarily attributable to the chlorophyll component, while betacyanin substantially contributes to extending the absorption spectrum at 550 nm. The combination of these two dyes in the cocktail improves the overall absorption efficiency. The synergistic effect of both dyes enhances light capture across the spectrum, particularly at the 660 nm peak dominated by chlorophyll, as well as at other wavelengths. This broad and intensified absorption profile promotes more efficient photon utilization and sustained electron generation.

Table 1. The peaks observed and their corresponding vibration mode.

Peak Position (cm^{-1})	Sample(s) Observed	Vibration Mode	Interpretation and Significance	References
2950–2700	(a) and (c)	CH_2 symmetric and asymmetric stretch	Broad in pure PEO; narrows in (c), indicating restricted chain motion due to graphite interaction.	(Tsai et al., 2004) (Nethravathi & Rajamathi, 2008)
1600–1500	(b), (a) and (c)	C=C stretching (graphite, PEO)	Present in graphite and seen in (c), confirming successful incorporation.	(Szabó et al., 2006) (Chen et al., 2015)
1150–1050	(a), (c)	C–O–C symmetric stretching	Becomes broader and intense in (c), showing increased polymer-filler interaction.	(Gómez et al., 2021) (Arulsankar et al., 2013)
~900–700	(c)	Graphite peaks	New sharp peaks appear, attributed to structural modes of graphite within the PEO matrix.	(Park et al., 2009)

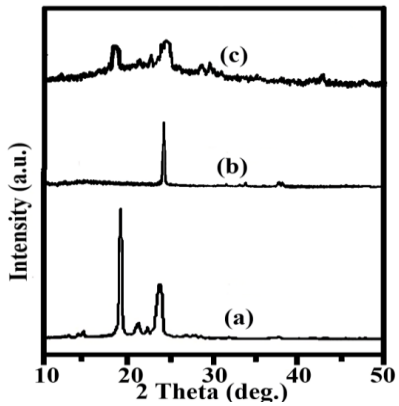

Figure 6. XRD of (a) Pure PEO, (b) Pure Graphite, and (c) 98 {80 PEO- 20 LiI: I_2}: 2 graphite

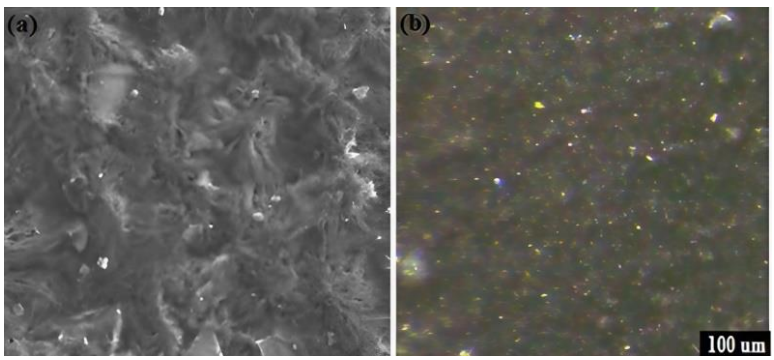

Figure 7. Optical micrograph of the polymer electrolyte film (a) pure PEO (b) 98 {80 PEO- 20 LiI: I_2}: 2 graphite

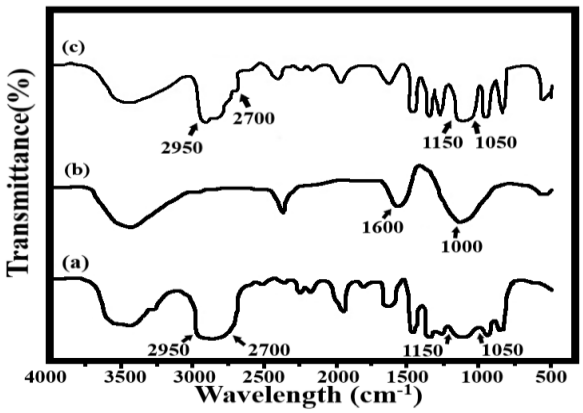

Figure 8. FTIR of (a) Pure PEO, (b) Graphite and (c) 98 {80 PEO- 20 LiI: I_2}: 2 graphite

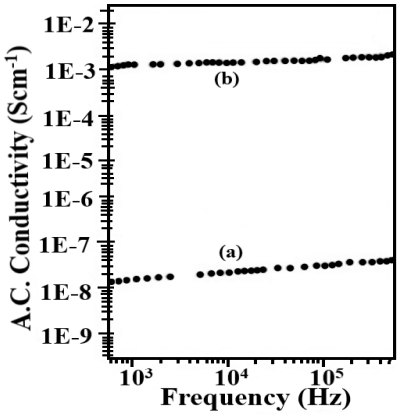

Figure 9. Variation of ac conductivity of the films with frequency (a) Pure PEO and (b) 98 {80 PEO- 20 LiI: I_2}: 2 graphite

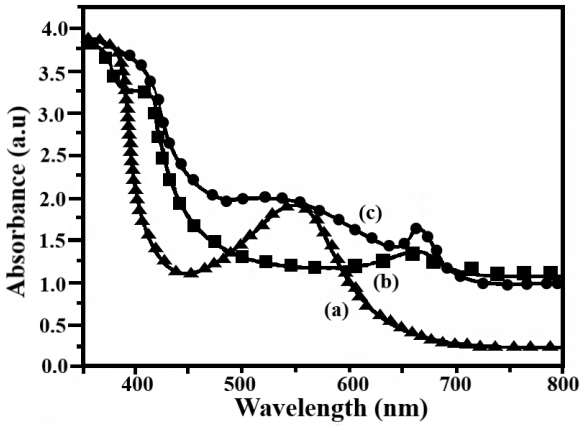

Figure 10. Absorption spectra of dyes: (a) *Spinacia oleracea* dye, (b) *Beta vulgaris* dye, and (c) Cocktail dye

The behavior of TiO_2–CuO photoelectrodes coated with the cocktail dye is shown in Figure 11. The enhanced interaction between TiO_2–CuO and the cocktail dye is likely responsible for the observed improvement in the light absorption range, as it facilitates charge transfer and reduces the recombination rate. CuO acts as an electron-accepting species, which enhances the photocatalytic performance of TiO_2. Additionally, the suitable conduction band alignment of CuO allows efficient transfer of photogenerated electrons from TiO_2, thereby promoting effective charge separation.

Figure 12 shows the XRD pattern of the synthesized TiO_2–CuO nanocomposite. The data indicate that the resulting nanoparticles are crystalline and do not contain any amorphous phases. Furthermore, the XRD pattern confirms that no new phases or compounds were formed during the synthesis.

The SEM (scanning electron microscopy) image of the synthesized TiO_2–CuO nanocomposite is shown in Figure 13. The image reveals a nanocrystalline structure of the composite. Using SEM analysis in combination with Scherrer's equation applied to the diffraction peaks, the average grain size was estimated to be 20–35 nm.

The small grain size provides a large surface area for dye adsorption, which can contribute to higher DSSC efficiency. The SEM image also indicates that CuO is distributed over the TiO_2 surface in the form of islands rather than forming a new compound. The increased photoactive surface area resulting from the nanocrystalline morphology is expected to enhance the overall efficiency of the solar cell.

Figure 14 illustrates the performance of PEO-based DSSCs, both with and without graphite as a filler, using a TiO_2–CuO photoelectrode sensitized with the cocktail dye. Comparative analysis shows that the DSSC incorporating graphite exhibits higher efficiency. The presence of graphite enhances the conductivity of the polymer electrolyte and improves overall cell performance, likely due to more efficient electron transport within the electrolyte. Table 2 presents a comparative study detailing key performance metrics, including power conversion efficiency, fill factor, and short-circuit current density, for the fabricated DSSCs.

Previous studies have explored various strategies to enhance the efficiency and stability of DSSCs by modifying key components such as the electrolyte, sensitizer, and

photoanode. Approaches have included doping polymer electrolytes with organic additives, ionic liquids, or nanofillers, as well as introducing advanced dyes or co-sensitizers to broaden the absorption spectrum. For instance, incorporation of 4-nitroaniline (Sathya et al., 2025) and Al_2O_3 nanofillers (Kim et al., 2024) improved ionic conductivity and overall efficiency, while co-sensitization with POBA and Z907 dyes (Devadiga et al., 2022) significantly enhanced light absorption and device performance.

However, many of these systems rely on costly or synthetic materials. In contrast, the present study introduces a sustainable approach by combining a natural cocktail dye, a graphite-reinforced PEO-based polymer electrolyte, and a TiO_2–CuO nanocomposite photoanode. This eco-friendly configuration achieved a power conversion efficiency of 3.3% with a fill factor of 57%, demonstrating a favorable balance among performance, cost, and environmental compatibility. A detailed comparative summary of these studies is presented in Table 3.

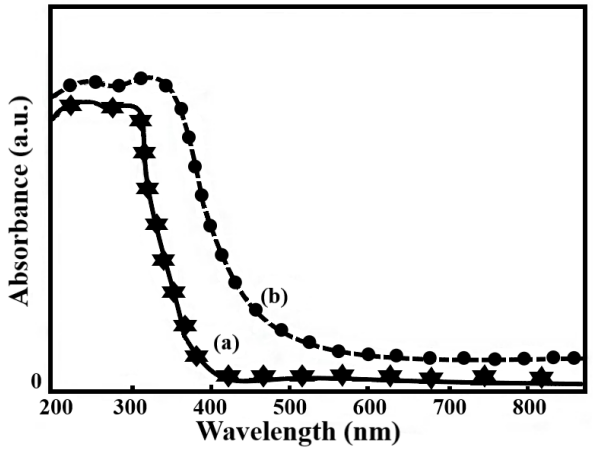

Figure 11. Absorption spectra of cocktail dye coated photoelectrode on ITO glass substrate (a) TiO_2 (b) TiO_2-CuO

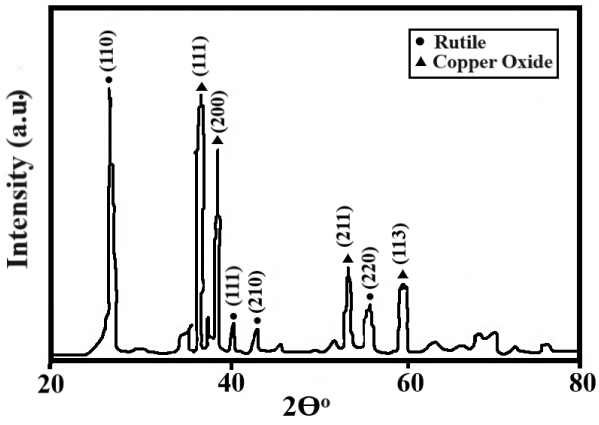

Figure 12. XRD pattern of TiO_2-CuO nanopowder

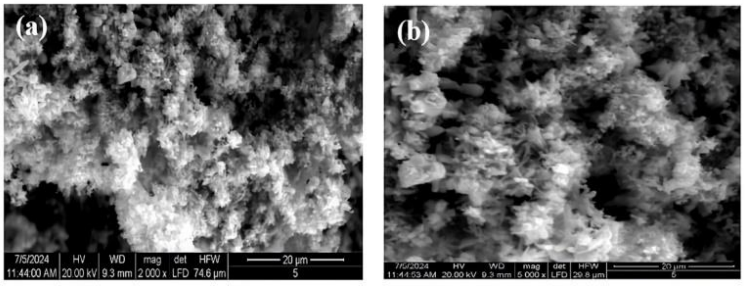

Figure 13. Scanning Electron Micrograph of (a) ns- TiO_2 (b) ns- TiO_2-CuO

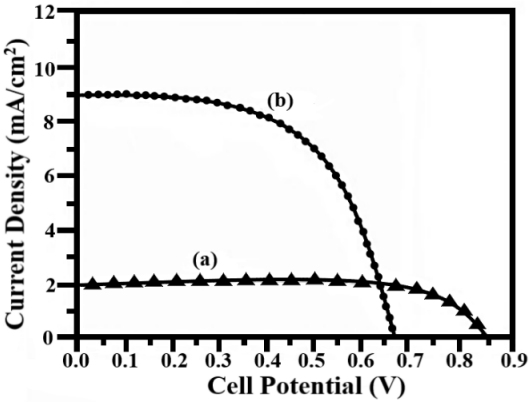

Figure 14. J-V characteristic curve of cocktail dye coated TiO_2-CuO photoelectrode (a) PEO: LiI/I_2 (b) 98 {80 PEO- 20 LiI: I_2}: 2 graphite

Table 2. Comparative study of DSSCs based on PEO with and without graphite filler

S.No.	Electrolyte System	I_{sc},(mA/cm^2)	V_{oc}, (V)	FF, %	η, (Efficiency)
1.	PEO: LiI/I_2	2.0	0.82	63	1.06%
2.	PEO: LiI/I_2/Graphite	9.0	0.68	57	3.3%

Table 3. A Comparative analysis of the present study with previously reported work.

S.No.	Electrolyte System	Dye	Photoanode Material	Counter Electrode	Efficiency (%)	Reference
1	PVA–PVP + TBAI blend polymer electrolyte	Carbazole-based dye	Ag–TiO_2 (4%)	Pt & rGO	2.37 (Pt), 1.06 (r-GO)	(Devadiga et al., 2021)
2	PVDF–PEG + 1-n-hexyl-3-methylimidazolium iodide (GPE)	POBA, Z907, POBA+Z907	Ni–TiO_2 (4%)	Pt	1.85 (POBA), 4.52 (Z907), 5.77 (co-sensitized)	(Devadiga et al., 2022)
3	Polymer composite electrolyte with Al_2O_3 nanofiller	Synthetic Dye	TiO_2	Pt	5.61	(Kim et al., 2024)
4	PVDF-co-HFP + PMMA + Phenothiazine + I^-/I_3^-	Synthetic Dye	TiO_2	Pt	5.20	(Subramanian et al., 2024)
5	Gelatin-based gel electrolyte + SAA additive	Synthetic Dye	TiO_2	Pt	5.8 (SAA), 3.9 (GLN)	(Devikala & Abisharani, 2024)
6	Chitosan + KI + PMII + Polyaniline (Quasi-solid Electrolyte)	Synthetic Dye	TiO_2	Pt	0.058	(Hatmanto et al., 2025)
7	PVDF + LiI + I_2 + 30% 4-Nitroaniline (SPE)	Synthetic Dye	TiO_2	Pt	3.73	(Sathya et al., 2025)
8	PEO + LiI/I_2 + EC + PC + graphite (SPE, solution-cast)	Natural Cocktail of beetroot & spinach (1:1 v/v)	TiO_2-CuO	Pt	3.3	Current Study

4. CONCLUSIONS

In this study, a natural dye-sensitized solar cell was successfully fabricated using a PEO-based polymer electrolyte, both with and without graphite filler, and a CuO-modified TiO_2 photoanode. The photovoltaic performance of the DSSC was significantly enhanced by incorporating 2 wt% graphite into the PEO:LiI/I_2 matrix. The power conversion efficiency (PCE) increased from 1.06% (without graphite) to 3.3% (with graphite), corresponding to an efficiency improvement of approximately 211%, as calculated using the formula:

$$\frac{3.3 - 1.06}{1.06} \text{ X } 100 \approx 211\%$$

This substantial increase indicates that the graphite filler effectively enhances ionic conductivity and restricts polymer chain mobility by reinforcing polymer–filler interactions, as also evidenced in the FTIR spectra. Additionally, surface modification of TiO_2 with CuO created an interfacial energy barrier that suppressed recombination losses, while the use of the cocktail dye improved charge transfer efficiency and light-harvesting capability. Collectively, these synergistic effects produced a more efficient, stable, and high-performing DSSC system based on environmentally benign materials.

5. ACKNOWLEDGEMENT

The authors gratefully acknowledge the Council of Science and Technology, Uttar Pradesh (CSTUP), for providing financial support.

REFERENCES

1. Anucha, C. B., Altin, I., Bacaksiz, E., & Stathopoulos, V. N. (2022). Titanium dioxide (TiO_2)-based photocatalyst materials activity enhancement for contaminants of emerging concern (CECs) degradation: In the light of modification strategies. Chemical Engineering Journal Advances, 10, 100262. https://doi.org/10.1016/j.ceja.2022.100262.

2. Arulsankar, A. N., Kulasekara, P., Jeya, S., Jayanthi, S., & Balakrishnan, S. (2013). Investigation of the structural, electrical and morphological properties of Mg^{2+} ion conducting nanocomposite solid polymer electrolytes based on PMMA. *International Journal of Innovative Research in Science, Engineering and Technology, 2*(12), 4883. https://www.researchgate.net/publication/257133066

3. Bathaei, S. A. H., Iranmanesh, M., Amiri, H., & Kourki, H. (2022). Investigation of the enhancement of thermophysical properties of new combinations of MWCNTs with several PCMs consisting of a type of paraffin in comparison with some mineral compounds (AN-MN-6H_2O). Journal of Renewable Energy and Environment. https://doi.org/10.30501/jree.2022.339549.1363

4. Cermak, M., Perez, N., Collins, M., & Bahrami, M. (2020). Material properties and structure of natural graphite sheet. Scientific Reports, 10, 18672. https://doi.org/10.1038/s41598-020-75393-y

5. Chawla, P., Pooja, K., & Tripathi, M. (2022). PVDF-based nanocomposite polymer electrolyte for enhancement in stability of dye-sensitized solar cells. Proceedings of the National Workshop on Recent Advances in Condensed Matter and High Energy Physics, 278, 121–129. https://doi.org/10.1007/978-981-19-2592-4_15

6. Chen, X., Lai, X., Hu, J., & Wan, L. (2015). An easy and novel approach to prepare Fe_3O_4-reduced graphene oxide composite and its application for high-performance lithium-ion batteries. *RSC Advances, 5*(86), 70408–70415. https://doi.org/10.1039/C5RA07347B

7. Coetzee, D., Militký, J., Wiener, J., & Venkataraman, M. (2023). Comparison of the synthesis, properties, and applications of graphite, graphene, and expanded graphite. Advanced Structured Materials, 201, 71–87. https://doi.org/10.1007/978-981-99-6002-6_4

8. Devadiga, D., Selvakumar, M., Devadiga, D., Ahipa, T. N., Shetty, P., Paramasivam, S., & Kumar, S. S. (2022). Synthesis and characterization of a new phenothiazine-based sensitizer/co-sensitizer for efficient dye-sensitized solar cell performance using a gel polymer electrolyte and Ni–TiO_2 as a photoanode. New Journal of Chemistry. https://doi.org/10.1039/D2NJ03589H

9. Devadiga, D., Selvakumar, M., Shetty, P., Mahesha, M. G., Devadiga, D., Ahipa, T. N., Kumar, S., & Hide. (2021). Novel photosensitizer for dye-sensitized solar cell based on ionic liquid–doped blend polymer electrolyte. *Journal of Solid State Electrochemistry, 25*(30), 1–18. https://doi.org/10.1007/s10008-021-04920-2

10. Devikala, S., & Abisharani, J. M. (2024). Addition of organic compounds in gelatin-biopolymer gel electrolyte for enhanced dye-sensitized solar cells. *IntechOpen*. https://doi.org/10.5772/intechopen.1003045

11. Dissanayake, M. A. K. L., Ekanayake, E. M. B. S., Bandara, L. R. A. K., Seneviratne, V. A., Thotawatthage, C. A., Jayaratne, S. L., & Senadeera, G. K. R. (2016). Efficiency enhancement by mixed cation effect in polyethylene oxide (PEO)-based dye-sensitized solar cells. Journal of Solid-State Electrochemistry, 20, 193–201. https://doi.org/10.1007/s10008-015-3018-1

12. Dissanayake, M. A. K. L., Rupasinghe, W. N. S., Seneviratne, V. A., Thotawatthage, C. A., & Senadeera, G. K. R. (2024). Efficiency enhancement due to the combined mixed cation effect and TiO_2 nanofiller effect in PEO and ionic liquid-based dye-sensitized solar cells. Journal of Solid State Electrochemistry, 28, 2561–2571. https://doi.org/10.1007/s10008-023-05797-z

13. Gómez, I. J., Vázquez Sulleiro, M., Mantione, D., & Alegret, N. (2021). Carbon nanomaterials embedded in conductive polymers: A state of the art. *Polymers, 13*(5), 745. https://doi.org/10.3390/polym13050745

14. Grätzel, M. (2001). Photoelectrochemical cells. Nature, 414, 338–344. https://doi.org/10.1038/35104607

15. Hao, S.-M., Zhu, J., He, S., Ma, L., Liu, W., Zhang, Y., Xie, X., Qin, X., Fan, X., Li, H., Zhang, L., & Zhou, W. (2024). Water-in-polymer electrolyte with a wide electrochemical window and recyclability. Nature Sustainability, 7, 661–671. https://doi.org/10.1038/s41893-024-01327-5

16. Hatmanto, A. D., Puspitaningrum, I., Tefa, Y. N. C., Santosa, S. J., & Kartini, I. (2025). Toward eco-friendly dye-sensitized solar cells: Developing chitosan-based electrolytes with conducting polymers and ionic liquids. International Journal of Renewable Energy Development. https://doi.org/10.61435/ijred.2025.61085.

17. Hebali, M., Ibari, B., Bennaoum, M., Beyour, M. E. A., Berka, M., Azzeddine, H. A., & Maachou, A. (2024). Electrical properties of ITO/$Al_{0.7}Ga_{0.3}As$/ITO solar cell with and without defects. Journal of Renewable Energy and Environment. https://doi.org/10.30501/jree.2024.408179.1632.

18. Ida, J., & Suthanthiraraj, S. A. (2019). Investigation on the effect of nitrogenous compound benzotriazole on the structural, thermal, and dielectric properties of PEO-PMMA blended polymer electrolyte system and its performance in dye-sensitized solar cells. Macromolecular Research, 27, 346–353. https://doi.org/10.1007/s13233-019-7056-x.

19. Khan, H., & Shah, M. U. H. (2023). Modification strategies of TiO_2-based photocatalysts for enhanced visible light activity and energy storage ability: A review. Journal of Environmental Chemical Engineering, 11(6), 111532. https://doi.org/10.1016/j.jece.2023.111532.

20. Khan, M. W., & Sahai, R. S. N. (2024). Analysis of accelerated weathering and mechanical properties of HDPE polymer composites with carbon black and zinc oxide nanoparticles for floating solar power plants. Journal of Renewable Energy and Environment. https://doi.org/10.30501/jree.2024.425816.1737.

21. Kim, E.-B., Kim, T.-G., Akhtar, M. S., Umar, A., Fouad, H., Abd El-Salam, N. M., & Ameen, S. (2024). Enhanced performance of dye sensitized solar cells through the incorporation of Al_2O_3 nanofillers in polymer electrolytes. *Science of Advanced Materials, 16*(2), 159–166. https://doi.org/10.1166/sam.2024.4650

22. Kohestani, H. R., & Ezoji, R. (2021). Synthesis and characterization of TiO_2/CuO/WO_3 ternary composite and its application as photocatalyst. International Journal of Engineering, 34(3C), 721–727. https://doi.org/10.5829/IJE.2021.34.03C.17.

23. Krishnan, A., Swarnalal, A., Das, D., Krishnan, M., Saji, V. S., & Shibli, S. M. A. (2024). A review on transition metal oxides based photocatalysts for degradation of synthetic organic pollutants. Journal of Environmental Sciences, 139, 389–417. https://doi.org/10.1016/j.jes.2023.02.051.

24. Lu, X., Wang, Y., Xu, X., Yan, B., Wu, T., & Lu, L. (2023). Polymer-based solid-state electrolytes for high-energy-density lithium-ion batteries – Review. Advanced Energy Materials, 13(38), Article 202301746. https://doi.org/10.1002/aenm.202301746.

25. Lv, H., Chu, X., Zhang, Y., Liu, Q., Wu, F., & Mu, D. (2024). Self-healing solid-state polymer electrolytes for high-safety and long-cycle lithium-ion batteries. Materials Today, 78, 181–208. https://doi.org/10.1016/j.mattod.2024.06.018

26. Mao, C., Wood, M., David, L., An, S. J., Sheng, Y., Du, Z., Meyer, H. M. III, Ruther, R. E., & Wood, D. L. III. (2018). Selecting the best graphite for long-life, high-energy Li-ion batteries. Journal of The Electrochemical Society, 165(9), A1837. https://doi.org/10.1149/2.1111809jes

27. Nethravathi, C., & Rajamathi, M. (2008). Chemically modified graphene sheets produced by the solvothermal reduction of colloidal dispersions of graphite oxide. Carbon, 46, 1994–1998. https://doi.org/10.1016/j.carbon.2008.08.013

28. Nei de Freitas, J., Nogueira, A. F., & de Paoli, M.-A. (2009). New insights into dye-sensitized solar cells with polymer electrolytes. Journal of Materials Chemistry, 19, 5279–5294. https://doi.org/10.1039/B900928K

29. Ngai, K. S., Ramesh, S., Ramesh, K., & Juan, J. C. (2016). A review of polymer electrolytes: Fundamental, approaches and applications. Ionics, 22(5), 1259–1279. https://doi.org/10.1007/s11581-016-1756-4

30. Nogueira, A. F., Durrant, J. R., & de Paoli, M. A. (2001). Dye-sensitized nanocrystalline solar cells employing a polymer electrolyte. Advanced Materials, 13, 826–830. https://doi.org/10.1002/1521-4095(200106)13:11%3C826::AID-ADMA826%3E3.0.CO;2-L

31. Park, S., & Ruoff, R. S. (2009). Chemical methods for the production of graphenes. Nature Nanotechnology, 4, 217–224. https://doi.org/10.1038/nnano.2009.58

32. Pooja, K., Chawla, P., & Tripathi, M. (2021). PVA-based polymer electrolyte with layered filler graphite for natural dye-sensitized solar cell. Nanoscience and Materials Science, 3(1). https://doi.org/10.30564/nmms.v3i1.3301

33. Pooja, K., Tripathi, M., & Chawla, P. (2022). Efficient natural dye-sensitized solar cell from PVDF-based polymer electrolyte filled with layered graphite. International Journal of Materials Research, 113. http://dx.doi.org/10.1515/ijmr-2021-8638

34. Sangwan, B., Kumar, S., Singh, A., Pandey, S. P., Singh, P. K., Singh, R. C., & Tomar, R. (2023). Modified poly(vinyl alcohol)-based polymer electrolyte for dye-sensitized solar cells (DSSCs). Macromolecular Symposia, 407, 2100462. https://doi.org/10.1002/masy.202100462

35. Sathya, K., Janet, D., & Kotteswaran, S. (2025). Effect of 4-nitroaniline-doped PVDF/LiI/I_2 based polymer electrolyte for dye sensitized solar cell applications. Journal of Materials Science: Materials in Electronics, 36, 1038. https://doi.org/10.1007/s10854-025-15055-9

36. Shin, C. K., Paek, Y.-K., & Lee, H.-J. (2006). Effect of CuO on the sintering behaviour and dielectric characteristics of titanium dioxide. International Journal of Applied Ceramic Technology, 3(4), 463–469. https://doi.org/10.1111/j.1744-7402.2006.02106.x

37. Shriver, D. F., Papke, B. L., Ratner, M. A., Dupon, R., Wong, T., & Brodwin, M. (1981). Structure and ion transport in polymer-salt complexes. Solid State Ionics, 5, 83–88. https://doi.org/10.1016/0167-2738(81)90199-5

38. Subramanian, A., Murugapoopathi, S., & Amesho, K. T. T. (2024). Enhancing the performance of nanocrystalline TiO_2 dye-sensitized solar cells with phenothiazine-doped blended solid polymer electrolyte. Electrocatalysis, 15, 226–238. https://doi.org/10.1007/s12678-024-00867-w

39. Szabó, T., Berkesi, O., Forgó, P., Josepovits, K., Sanakis, Y., Petridis, D., & Dékány, I. (2006). Evolution of surface functional groups in a series of progressively oxidized graphite oxides. *Chemistry of Materials, 18*(11), 2740–2749. https://doi.org/10.1021/cm060258

40. T. K., & Saratha, R. (2024). Natural polymer-based electrolytes for energy storage devices—an overview. Ionics, 30, 1245–1266. https://doi.org/10.1007/s11581-023-05315-1

41. Tripathi, M., & Chawla, P. (2015). CeO_2–TiO_2 photoanode for solid-state natural dye-sensitized solar cell. Ionics, 21(3), 541. https://doi.org/10.1007/s11581-014-1172-6

42. Tsai, J.-C., Lo, Y.-L., Lin, C.-Y., Sheu, H., & Lin, J.-C. (2004). Feasibility of rapid quantitation of stratum corneum lipid content by Fourier transform infrared spectrometry. Journal of Spectroscopy, 18. https://doi.org/10.1155/2004/401015

43. Wen, S. J., Richardson, T. J., Ghantous, D. I., Striebel, K. A., Ross, P. N., & Cairns, E. J. (1996). FTIR characterization of PEO + $LiN(CF_3SO_2)_2$ electrolytes. Journal of Electroanalytical Chemistry, 408, 113–118. https://doi.org/10.1016/0022-0728(96)04536-6

44. Zhang, H., Yang, Y., Ren, D., Wang, L., & He, X. (2021). Graphite as anode materials: Fundamental mechanism, recent progress and advances. Energy Storage Materials, 36, 147–170. https://doi.org/10.1016/j.ensm.2020.12.027

45. Zhao, Y., Wang, L., Zhou, Y., Liang, Z., Tavajohi, N., Li, B., & Li, T. (2021). Solid polymer electrolytes with high conductivity and transference number of Li ions for Li-based rechargeable batteries. Advanced Science, 8, 2003675. https://doi.org/10.1002/advs.202003675